

Reversal of quantised Hall drifts at non-interacting and interacting topological boundaries

Zijie Zhu,^{*} Marius Gächter,^{*} Anne-Sophie Walter, Konrad Viebahn,[†] and Tilman Esslinger
Institute for Quantum Electronics & Quantum Center, ETH Zurich, 8093 Zurich, Switzerland

The transport properties of gapless edge modes at boundaries between topologically distinct domains are of fundamental and technological importance. Therefore, it is crucial to gain a better understanding of topological edge states and their response to interparticle interactions. Here, we experimentally study long-distance quantised Hall drifts in a harmonically confined topological pump of non-interacting and interacting ultracold fermionic atoms. We find that quantised drifts halt and reverse their direction when the atoms reach a critical slope of the confining potential, revealing the presence of a topological boundary. The drift reversal corresponds to a band transfer between a band with Chern number $C = +1$ and a band with $C = -1$ via a gapless edge mode, in agreement with the bulk-edge correspondence for non-interacting particles. We establish that a non-zero repulsive Hubbard interaction leads to the emergence of an additional edge in the system, relying on a purely interaction-induced mechanism, in which pairs of fermions are split.

The existence of individual edge modes at topological boundaries plays a crucial role in quantum Hall physics. More specifically, a non-trivial topology in the bulk of a material ensures that its edge modes are gapless and chiral. Gaplessness is related to the bulk-edge correspondence, stating that the number of topological edge modes is equal to the difference in Chern number across an interface [1]. Consequently, a gapless mode should allow an adiabatic transfer from one band to another, resulting in a reflection of transverse bulk currents in the opposite direction if the two bands feature opposite Chern numbers. However, the coherence time in most electronic materials is not sufficient to observe this effect, and edges are generally probed spectroscopically [1–4]. Moreover, studies of edge physics in engineered quantum systems, such as ultracold atoms and photonics, have so far been focussed on chirality [5–9] and localisation [10–13]. A boundary reflection has not been detected [14, 15], or it was disregarded [16, 17], and to our knowledge it has never been studied for variable interaction strength. Here, we observe the reversal of quantised bulk drifts due to harmonic trapping in a topological Thouless pump, the temporal analogue of the quantum Hall effect [18–20]. The reflection is a fundamental manifestation of confined topological matter and directly shows the gapless nature of topological edge modes. Going beyond the non-interacting regime, we discover the emergence of a second edge for repulsive Hubbard U .

The experiments are performed with ultracold fermionic potassium-40 atoms, which are loaded into the potential of a generalised optical lattice formed by a combination of standing and running waves of wavelength $\lambda = 1064 \text{ nm}$ [22]. This creates an array of decoupled, one-dimensional tubes. Along the tube direction, the periodically modulated Rice-Mele-Hubbard Hamiltonian

with harmonic confinement is realised,

$$\begin{aligned} \hat{H}(\tau) = & - \sum_{j,\sigma} [t + (-1)^j \delta(\tau)] \left(\hat{c}_{j\sigma}^\dagger \hat{c}_{j+1\sigma} + \text{h.c.} \right) \quad (1) \\ & + \Delta(\tau) \sum_{j,\sigma} (-1)^j \hat{c}_{j\sigma}^\dagger \hat{c}_{j\sigma} + U \sum_j \hat{c}_{j\uparrow}^\dagger \hat{c}_{j\uparrow} \hat{c}_{j\downarrow}^\dagger \hat{c}_{j\downarrow} \\ & + \sum_{j,\sigma} V_j \hat{c}_{j\sigma}^\dagger \hat{c}_{j\sigma}, \end{aligned}$$

where $\hat{c}_{j\sigma}$ is the fermionic annihilation operator for spin $\sigma \in \{\uparrow, \downarrow\}$ on site j , and t denotes the average tunnelling. An adiabatic modulation of bond dimerisation $\delta(\tau) = \delta_0 \cos(2\pi\tau/T)$ and sublattice offset $\Delta(\tau) = \Delta_0 \sin(2\pi\tau/T)$ traces a closed trajectory in the δ - Δ plane around the origin, referred to as critical point. Therefore, an insulator or homogeneously filled band at $U = 0$ describes a topological pump [18, 20] with T being the pump period. Experimentally, the topological pump manifests itself as a quantised drift of the atom position by one unit cell per pump cycle [23–27].

The harmonic confinement is characterised by the trap frequency ν , entering Eq. 1 as $V_j = \frac{1}{2}m(2\pi\nu a_j)^2 \equiv V_0 j^2$ ($a = \lambda/2$, lattice spacing; m , atomic mass). Due to the confinement, the atoms are initially localised at the centre of the trap. Topological pumping then leads to a quantised drift of atoms against the confining potential (Fig. 1A). Our measurements show that the quantised drift changes its direction at a certain distance from the trap centre. We will demonstrate that this happens when the gradient of the confinement overcomes the band gap and a boundary between topological and trivial regions emerges. For repulsive interactions, we observe another reflection, closer to the trap centre, while a part of the atoms keeps drifting in the original direction (Fig. 1A).

In the following, we develop a description of the reflection in terms of gapless edge modes and the bulk-edge correspondence within the framework of the Harper-Hofstadter-Hatsugai (HHH) model with one real (x) and one synthetic (n) dimension. The model features bulk

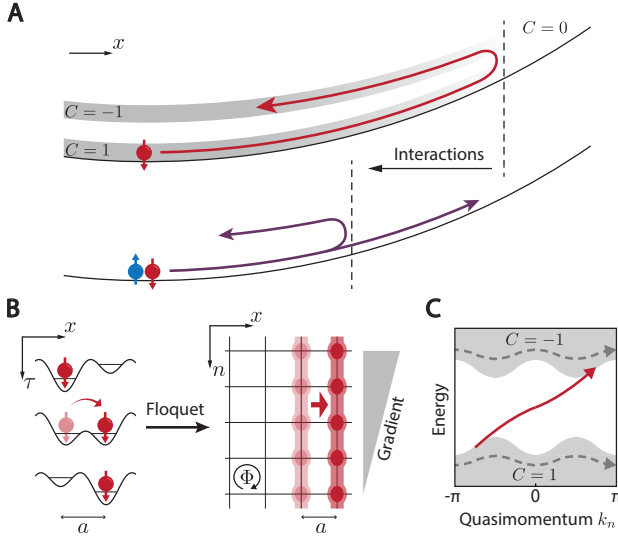


FIG. 1. Reflection of quantised Hall drifts off a topological interface. (A) Topological Thouless pumping in the presence of confining potentials. In the non-interacting case (top), a harmonic trap gives rise to topological trivial ($C = 0$) and non-trivial ($C \neq 0$) regions, separated by a topological interface. The atoms exhibit a quantised drift until they are reflected at the interface. With repulsive on-site interactions (bottom), the reflection happens closer to the centre, accompanied by atoms still drifting in the original direction. (B) Using Floquet theory, the 1D Rice-Mele pump can be mapped to a 2D Harper-Hofstadter-Hatsugai model with a linear gradient along the synthetic dimension n which represents the photon number. The magnetic flux per plaquette is $\Phi = 1/2$ in units of the magnetic flux quantum [21]. The gradient along n leads to a transverse Hall drift along x (red arrows) due to the nontrivial topology of the bands. (C) Schematic spectrum of the mapped 2D Hofstadter model in a semi-infinite geometry. The lowest two bands have $C = \pm 1$, respectively. The linear gradient induces Bloch oscillations in the synthetic reciprocal space (dashed arrows). A gapless edge mode (solid arrow) appears at the topological interface. The reflection of the Hall drift can be understood as atoms being transported from the lower band ($C = 1$) to the higher band ($C = -1$) via the topological edge mode.

Chern bands with $C = +1$ and $C = -1$. An exact mapping between the non-interacting 1D Rice-Mele Hamiltonian (Eq. 1) and the two-dimensional (2D) HHH model can be obtained using Floquet theory, illustrated in Fig. 1B (for derivation see, e.g., refs. [19] and [21]). A linear gradient along the synthetic dimension n appears in the mapping since the state with n photons acquires an energy of $-n\hbar\omega$, where $\omega = 2\pi/T$ is the pump frequency. The gradient along n or, equivalently, an external force causes Bloch oscillations along the synthetic reciprocal dimension k_n which, in turn, lead to a Hall drift or ‘anomalous velocity’ along the transverse real direction x [14, 15]. The bulk Hall drift along x corresponds exactly to the quantised displacement measured in the topological pump. The trap induces a boundary between

topological ($C_{\text{centre}} = 1$) and trivial ($C_{\text{right}} = 0$) regions and a single gapless edge mode emerges, according to the bulk-edge correspondence: $C_{\text{centre}} - C_{\text{right}} = 1$. The edge modes connects two bands of opposite Chern invariant, as shown in Fig. 1C. Thus, a Bloch oscillation transfers the atoms from the ground to the first excited band via that edge mode. Since the first excited band has Chern number -1 the atoms are now moving ‘backwards’, resulting in a reversal of the quantised Hall drift.

Fig. 2 shows experimental in-situ images of the atomic cloud as a function of time τ at $U = 0$. The data shows a quantised drift of $1.00(1) \times 2a/T$ up to about $60T$, which confirms the long coherence time of Bloch oscillations which induce the transverse drift. At $\tau \simeq 75T$ the atoms change their drift direction, which is a key observation of this work. The expected topological boundary (red dashed line) represents the position at which the local tilt from the external harmonic potential $\Delta_{\text{ext}}(j) \equiv \frac{1}{2}|V_j - V_{j-1}| = V_0|j - \frac{1}{2}|$ equals the maximum sublattice offset Δ_0 , thus, $x_{\text{edge}}/(2a) \simeq \frac{1}{2}\Delta_0/V_0 = 92(7)$. Beyond this position the total sublattice offset ceases to change sign, rendering the region outside x_{edge} topologically trivial. The boundary caused by the harmonic confinement is not infinitely sharp, but smoothed over several lattice sites. This leads to a small T -dependence of the reflection position (Fig. S1), compared to its absolute value, and the calculation above should be understood as the outermost point of the reflective region. The reflected atoms exhibit a quantised drift of $-0.99(3) \times 2a/T$ in the opposite direction, in agreement with a transfer to the first excited band with $C = -1$. The linear relation between the position of topological boundary x_{edge} and the maximum sublattice offset Δ_0 is further confirmed by measuring the reflection in different lattices (Fig. S1). The reflection is observed under all parameter settings tested in this work, highlighting that the existence of the topological boundary is robust.

In addition to the reflection, we also observe a cloud of atoms temporarily remaining at the boundary before gradually dissolving. This process can be understood via the presence of topologically trivial edge states, which hybridise with the gapless edge modes. To simplify the picture, let us consider a sharp domain wall between $C = 1$ and $C = 0$ (Fig. 2C). According to the bulk-edge correspondence, the topologically nontrivial region contributes exactly one gapless mode whereas the trivial region can contribute gapped edge modes. Due to tunnel coupling at the interface, hybridisation takes place [34] and gaps on the order of the pump frequency $2\pi/T$ emerge. Bloch oscillations along k_n can now lead to non-adiabatic ‘Landau-Zener’ transfers between topological and trivial edge modes, causing an incomplete transfer to the higher band, and atoms remaining at the boundary. Subsequent Bloch oscillations will transfer atoms back into the topological domain, leading to the dissolu-

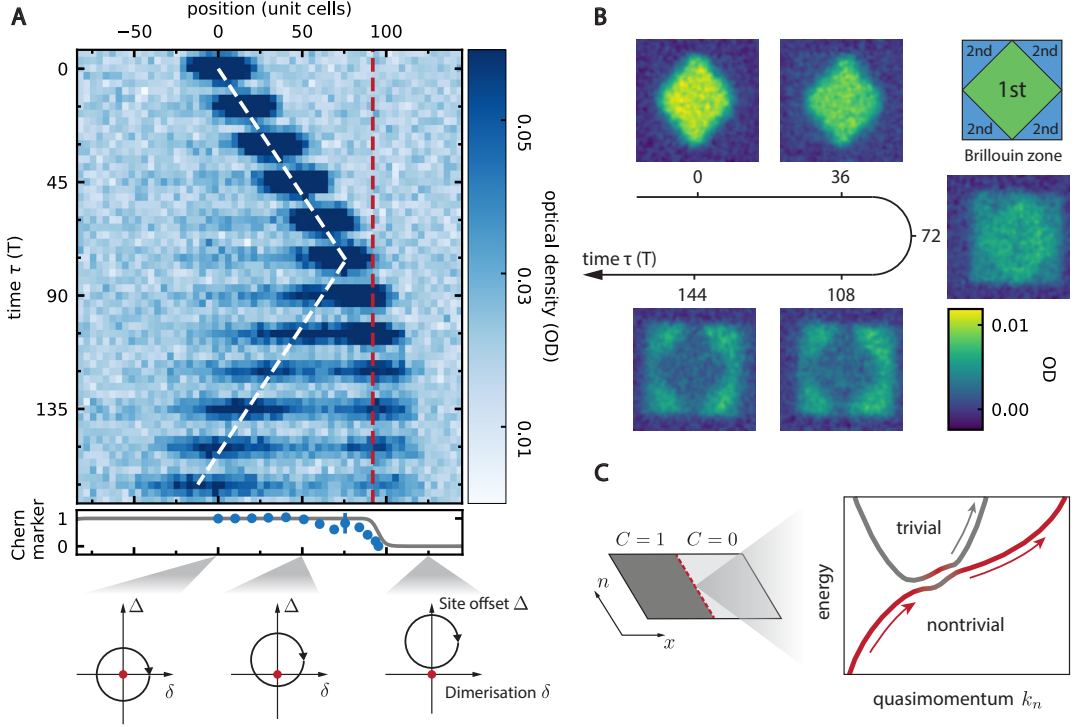


FIG. 2. Measuring the reversal of a quantised Hall drift. (A) The time-trace of atomic in-situ images shows a quantised drift along x before the atoms are reflected at the topological boundary. Each density image is averaged over three individual measurements with the parameters $V_0 = 0.0148(9)t$, $\Delta_0 = 2.7(1)t$, and $T = 3 \text{ ms} = 12.8(2)\hbar/t$. The red dashed line indicates the topological boundary $x_{\text{edge}}/(2a) \approx \frac{1}{2}\Delta_0/V_0$. The white dashed lines are linear fits to the atom drift, yielding slopes of $1.00(1) \times 2a/T$ before, and $-0.99(3) \times 2a/T$ after the reflection. Cloud positions, averaged over the transverse direction, are fitted using Gaussians. The experimental Chern marker (lower panel, points) is determined by the velocity of the right-moving cloud at different positions. The theoretical Chern marker (line) is calculated in a staggered potential $V_j = V_0(-1)^j j$ which has the same local tilt $\Delta_{\text{ext}}(j) = V_0 |j - \frac{1}{2}|$ as the harmonic trap [21]. In a local density approximation picture, the local tilt Δ_{ext} shifts the δ - Δ pump trajectory upwards. Depending on whether or not the trajectory encloses the critical point, the pump is rendered topological or trivial. (B) Measured band populations as a function of time τ . Each density image is averaged over six individual measurements with the parameters $V_0 = 0.0191(6)t$, $\Delta_0 = 3.2(2)t$ and $T = 3 \text{ ms} = 10.7(2)\hbar/t$. The total atom number remains constant, within error bars, throughout the experiment. Due to the underlying honeycomb lattice geometry in the x - z plane, the first Brillouin zone has a diamond shape [21]. The band population is inverted when the bulk current is reflected off the topological interface, manifesting the gapless nature of the topological edge mode. (C) Hybridisation of the edge modes at the topological interface due to tunnelling. Bloch oscillations along k_n can lead to Landau-Zener transfers between topologically trivial and nontrivial edge modes. The population of trivial edge modes explains the atoms being left at the boundary. Hybridisation never changes the total number of gapless edge modes at the boundary.

tion of the cloud at the boundary. While the harmonic confinement leads to a more complex level structure [21], the underlying process remains qualitatively the same.

We support the in-situ images with measurements of band population before, during, and after the reflection, as shown in Fig. 2B [21]. Before the reflection, we find a filled ground band, which is consistent with the observation of a quantised Hall drift. At the reflection ($\tau \simeq 72 T$), we observe an inversion of the population to the first excited band. After the reflection, the inverted population remains almost unchanged while the atoms are travelling back, highlighting the absence of incoherent relaxation to the ground band, even after more than a hundred Bloch oscillations.

We further explore the effect of attractive and repulsive interactions on the topological boundary. For attractive Hubbard $U = -3.48(7)t = 1.27(7)\Delta_0$ (Fig. 3A), the quantised Hall drift is reversed at the same position as in the non-interacting situation. This can be explained in terms of the Rice-Mele model in which fermions in the strongly attractive regime approach the limit of hard-core bosons [22], and the condition for the emergence of a topological boundary $\Delta_{\text{ext}}(j) = \Delta_0$ remains unchanged.

For repulsive Hubbard $U = 3.48(7)t$ (Fig. 3B), we observe a second reflection in addition to the original one. Compared to the non-interacting case, this reflection appears much closer to the trap centre. The zoomed-in image (Fig. 3C) shows that a proportion of the atoms start to move backwards after about 12 cycles. In con-

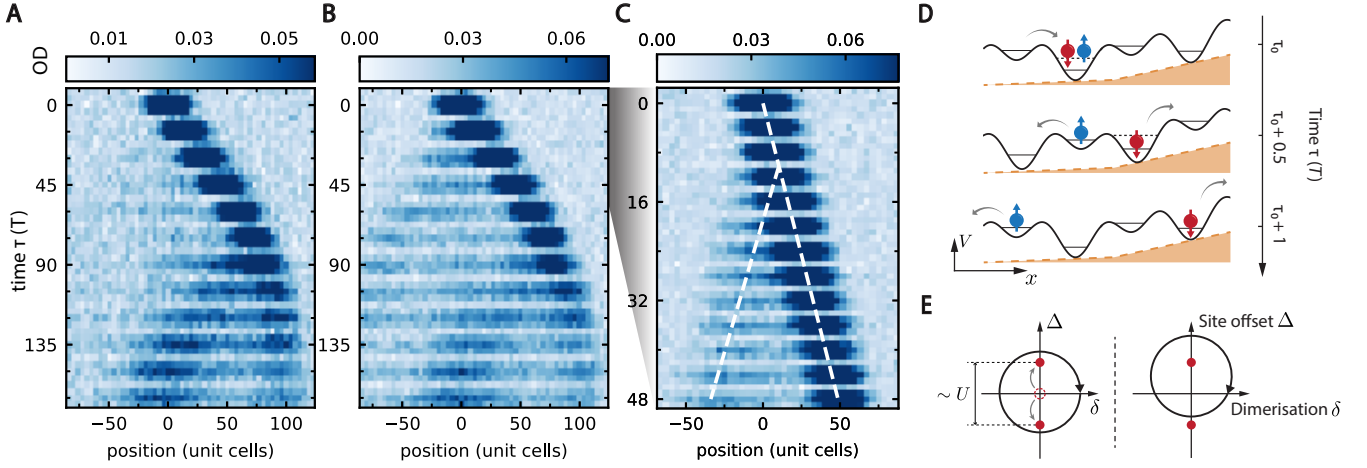


FIG. 3. Reflection of quantised Hall drifts from an interacting topological edge. (A) An attractive Hubbard interaction of $U = -3.48(7)t$ leads to the same reflection behaviour as observed for $U = 0$ (measurement parameters otherwise identical to Fig. 2A). (B) Repulsive Hubbard interactions of $U = 3.48(7)t$ lead to the emergence of a second reflection, closer to the trap centre, which we attribute to an interacting topological boundary. A zoom-in (C) shows that the early reflection happens after about twelve cycles. The white dashed lines are guides to the eye, calculated as linear fits to the cloud position, extracted as the sum of a skewed and a regular Gaussian. (D) Microscopic description of the interaction-induced reflection for repulsive Hubbard U . When the maximum energy offset between two neighbouring sites $2(\Delta_0 - \Delta_{\text{ext}})$ becomes smaller than the Hubbard interaction, formation of double occupancies is prohibited and one atom is left in the higher-energy site of a unit cell, which then drifts in the opposite direction. (E) The critical point in the δ - Δ plane is split into two in the presence of repulsive Hubbard U [35]. When the pump trajectory encloses both critical points, a quantised drift is expected, as in the non-interacting system. The local tilt given by the external potential Δ_{ext} shifts the trajectory along the Δ -axis, eventually enclosing just one critical point. Since a single split critical point features half the topological charge of the original one, the material's topology changes and a boundary emerges.

trast to the drift reversal in the non-interacting system, a large fraction of the atom cloud still undergoes quantised drifting in the original direction. In the following, we develop a microscopic picture of the interaction-induced partial reflection in the limiting case of two isolated spins (\uparrow, \downarrow), which approximates our initial state in a unit cell (Fig. 3D). As long as the maximum energy offset between two neighbouring sites $2(\Delta_0 - \Delta_{\text{ext}})$ is larger than the Hubbard U , the formation of a double occupancy is energetically allowed and the quantised drift persists [22], even in the presence of an external potential. However, when Δ_{ext} becomes larger, the energy offset between two neighbouring sites remains always smaller than U , double occupancy formation becomes prohibited. In the latter case, one atom of a singlet pair is transferred to the energetically excited site of a unit cell, which will subsequently drift in the opposite direction. The other atom, in the lower-energy site, will move onwards because on-site interactions become irrelevant if there is only one atom per unit cell. Since the underlying Hamiltonian (Eq. 1) is $\text{SU}(2)$ -symmetric, spin- \uparrow and spin- \downarrow have equal probability of being reflected and they should remain correlated after the splitting process.

The full many-body description of the interaction-induced reversal requires the development of suitable topological invariants for smooth confinements and strong interactions, which goes beyond the scope of this

work. Nevertheless, we obtain an intuition of the boundary's topological origins using again the idea of shifted pump trajectories in the δ - Δ plane with a staggered potential (c.f. Fig. 2A). Numerical simulations have shown that a repulsive Hubbard U can split the critical point at the origin into two separate ones [35], each retaining half the original topological charge. The distance between the new critical points is approximately U up to a correction on the order of the tunnelling t [36]. When the trajectory encloses both critical points, quantised drift of two spins (\uparrow, \downarrow) is expected, as in the non-interacting system. As the position-dependent local tilt $\Delta_{\text{ext}}(j)$ shifts the trajectory upwards, it will enclose only one of the critical points beyond certain position along x (Fig. 3E). This indicates a transition of topological properties and the emergence of an interacting topological edge in real space. The estimation of the interacting boundary at $\Delta_{\text{ext}}(j) \simeq \Delta_0 - U/2$ lies close to the centre and agrees with the microscopic picture discussed above. Similar to the non-interacting case, this boundary should be considered as the outermost position of the reflective region.

In conclusion, we have experimentally observed a reversal of quantised Hall drifts at a topological boundary in a harmonic potential. The reflection is a direct manifestation of the gapless nature of topological edge modes between Chern bands of opposite sign. We explore the effect of Hubbard interactions, both attractive and re-

pulsive, and find an asymmetric behavior with respect to $U = 0$. While on the attractive side the topological boundary is unaffected, repulsive interactions lead to the emergence of a second interface, featuring a splitting of quantised drifts. As a result, our experiments could enable the realisation of circular current patterns for constructing novel many-body phases [37]. More broadly, our work allows the exploration of the bulk-edge correspondence in the presence of interactions [38], as well as the investigation of edge reconstruction [39] in the quantum Hall effect and in interacting topological insulators.

ACKNOWLEDGMENTS

We would like to thank Jason Ho, Gian-Michele Graf, Thomas Ihn, Fabian Grusdt, Fabian Heidrich-Meisner, Armando Aligia, and Eric Bertok for valuable discussions. We also thank Julian Léonard and Nur Ünal for comments on an earlier version of the manuscript. We would like to thank Alexander Frank for his contributions to the electronic part of the experimental setup. We acknowledge funding by the Swiss National Science Foundation (Grant Nos. 182650, 212168, NCCR-QSIT, and TMAG-2 209376) and European Research Council advanced grant TransQ (Grant No. 742579).

* These authors contributed equally.

† viebahnk@phys.ethz.ch

- [1] M. Z. Hasan and C. L. Kane, *Colloquium: Topological insulators*, Rev. Mod. Phys. **82**, 3045 (2010).
- [2] M. Hafezi, S. Mittal, J. Fan, A. Migdall, and J. M. Taylor, Imaging topological edge states in silicon photonics, Nature Photon **7**, 1001 (2013).
- [3] K. Yatsugi, T. Yoshida, T. Mizoguchi, Y. Kuno, H. Iizuka, Y. Tadokoro, and Y. Hatsugai, Observation of bulk-edge correspondence in topological pumping based on a tunable electric circuit, Commun Phys **5**, 180 (2022).
- [4] Z.-C. Xiang, K. Huang, Y.-R. Zhang, T. Liu, Y.-H. Shi, C.-L. Deng, T. Liu, H. Li, G.-H. Liang, Z.-Y. Mei, H. Yu, G. Xue, Y. Tian, X. Song, Z.-B. Liu, K. Xu, D. Zheng, F. Nori, and H. Fan, Simulating quantum Hall effects on a superconducting quantum processor (2022), arXiv:2207.11797.
- [5] M. Atala, M. Aidelsburger, M. Lohse, J. T. Barreiro, B. Paredes, and I. Bloch, Observation of chiral currents with ultracold atoms in bosonic ladders, Nat Phys **10**, 1000 (2014).
- [6] B. K. Stuhl, H.-I. Lu, L. M. Ayccock, D. Genkina, and I. B. Spielman, Visualizing edge states with an atomic Bose gas in the quantum Hall regime, Science **349**, 1514 (2015).
- [7] M. Mancini, G. Pagano, G. Cappellini, L. Livi, M. Rider, J. Catani, C. Sias, P. Zoller, M. Inguscio, M. Dalmonte, and L. Fallani, Observation of chiral edge states with neutral fermions in synthetic Hall ribbons, Science **349**, 1510 (2015).
- [8] T. Chalopin, T. Satoor, A. Evrard, V. Makhalov, J. Dalibard, R. Lopes, and S. Nascimbene, Probing chiral edge dynamics and bulk topology of a synthetic Hall system, Nat. Phys. **16**, 1017 (2020).
- [9] T. Ozawa, H. M. Price, A. Amo, N. Goldman, M. Hafezi, L. Lu, M. C. Rechtsman, D. Schuster, J. Simon, O. Zilberberg, and I. Carusotto, Topological photonics, Reviews of Modern Physics **91**, 015006 (2019).
- [10] Y. E. Kraus, Y. Lahini, Z. Ringel, M. Verbin, and O. Zilberberg, Topological States and Adiabatic Pumping in Quasicrystals, Phys. Rev. Lett. **109**, 106402 (2012).
- [11] M. Leder, C. Grossert, L. Sitta, M. Genske, A. Rosch, and M. Weitz, Real-space imaging of a topologically protected edge state with ultracold atoms in an amplitude-chirped optical lattice, Nat Commun **7**, 13112 (2016).
- [12] E. J. Meier, F. A. An, and B. Gadway, Observation of the topological soliton state in the Su-Schrieffer-Heeger model, Nat Commun **7**, 13986 (2016).
- [13] F. A. An, E. J. Meier, and B. Gadway, Direct observation of chiral currents and magnetic reflection in atomic flux lattices, Sci. Adv. **3**, e1602685 (2017).
- [14] G. Jotzu, M. Messer, R. Desbuquois, M. Lebrat, T. Uehlinger, D. Greif, and T. Esslinger, Experimental realization of the topological Haldane model with ultracold fermions, Nature **515**, 237 (2014).
- [15] M. Aidelsburger, M. Lohse, C. Schweizer, M. Atala, J. T. Barreiro, S. Nascimbene, N. R. Cooper, I. Bloch, and N. Goldman, Measuring the Chern number of Hofstadter bands with ultracold bosonic atoms, Nature Physics **11**, 162 (2015).
- [16] Y. Qian, M. Gong, and C. Zhang, Quantum transport of bosonic cold atoms in double-well optical lattices, Phys. Rev. A **84**, 013608 (2011).
- [17] M. Bellec, C. Michel, H. Zhang, S. Tzortzakakis, and P. Delplace, Non-diffracting states in one-dimensional Floquet photonic topological insulators, EPL **119**, 14003 (2017).
- [18] N. R. Cooper, J. Dalibard, and I. B. Spielman, Topological bands for ultracold atoms, Reviews of Modern Physics **91**, 015005 (2019).
- [19] T. Oka and S. Kitamura, Floquet Engineering of Quantum Materials, Annu. Rev. Condens. Matter Phys. **10**, 387 (2019).
- [20] R. Citro and M. Aidelsburger, Thouless pumping and topology (2022), arXiv:2210.02050.
- [21] See supplemental materials, which include refs. [28–33].
- [22] A.-S. Walter, Z. Zhu, M. Gächter, J. Minguzzi, S. Roschinski, K. Sandholzer, K. Viebahn, and T. Esslinger, Quantisation and its breakdown in a Hubbard-Thouless pump (2022), arXiv:2204.06561 [cond-mat, physics:physics].
- [23] L. Wang, M. Troyer, and X. Dai, Topological Charge Pumping in a One-Dimensional Optical Lattice, Phys. Rev. Lett. **111**, 026802 (2013).
- [24] M. Lohse, C. Schweizer, O. Zilberberg, M. Aidelsburger, and I. Bloch, A Thouless quantum pump with ultracold bosonic atoms in an optical superlattice, Nature Physics **12**, 350 (2016).
- [25] S. Nakajima, T. Tomita, S. Taie, T. Ichinose, H. Ozawa, L. Wang, M. Troyer, and Y. Takahashi, Topological Thouless pumping of ultracold fermions, Nature Physics **12**, 296 (2016).
- [26] S. Nakajima, N. Takei, K. Sakuma, Y. Kuno, P. Marra, and Y. Takahashi, Competition and interplay between

- topology and quasi-periodic disorder in Thouless pumping of ultracold atoms, *Nat. Phys.* **17**, 844 (2021).
- [27] J. Minguzzi, Z. Zhu, K. Sandholzer, A.-S. Walter, K. Viebahn, and T. Esslinger, Topological Pumping in a Floquet-Bloch Band, *Phys. Rev. Lett.* **129**, 053201 (2022).
 - [28] J. K. Asbóth, L. Oroszlány, and A. Pályi, *A short course on topological insulators: band structure and edge states in one and two dimensions*, Lecture notes in physics Volume 919 (Springer, Cham, 2016).
 - [29] T. D. Stanescu, V. Galitski, and S. Das Sarma, Topological states in two-dimensional optical lattices, *Phys. Rev. A* **82**, 013608 (2010).
 - [30] M. Buchhold, D. Cocks, and W. Hofstetter, Effects of smooth boundaries on topological edge modes in optical lattices, *Phys. Rev. A* **85**, 063614 (2012).
 - [31] A. R. Kolovsky, F. Grusdt, and M. Fleischhauer, Quantum particle in a parabolic lattice in the presence of a gauge field, *Phys. Rev. A* **89**, 033607 (2014).
 - [32] N. Goldman, G. Jotzu, M. Messer, F. Görg, R. Desbuquois, and T. Esslinger, Creating topological interfaces and detecting chiral edge modes in a two-dimensional optical lattice, *Phys. Rev. A* **94**, 043611 (2016).
 - [33] R. Bianco and R. Resta, Mapping topological order in coordinate space, *Phys. Rev. B* **84**, 241106 (2011).
 - [34] A. Mook, J. Henk, and I. Mertig, Edge states in topological magnon insulators, *Phys. Rev. B* **90**, 024412 (2014).
 - [35] E. Bertok, F. Heidrich-Meisner, and A. A. Aligia, Splitting of topological charge pumping in an interacting two-component fermionic Rice-Mele Hubbard model, *Phys. Rev. B* **106**, 045141 (2022).
 - [36] M. E. Torio, A. A. Aligia, and H. A. Ceccatto, Phase diagram of the Hubbard chain with two atoms per cell, *Phys. Rev. B* **64**, 121105 (2001).
 - [37] F. Letscher, F. Grusdt, and M. Fleischhauer, Growing quantum states with topological order, *Phys. Rev. B* **91**, 184302 (2015).
 - [38] B. Irsigler, J.-H. Zheng, and W. Hofstetter, Interacting Hofstadter Interface, *Phys. Rev. Lett.* **122**, 010406 (2019).
 - [39] D. B. Chklovskii, B. I. Shklovskii, and L. I. Glazman, Electrostatics of edge channels, *Phys. Rev. B* **46**, 4026 (1992).

SUPPLEMENTAL MATERIALS

Dependence of the drift reversal on experimental parameters

The expected drift reversal happens when the maximum local site offset over one pump-cycle Δ_0 is equal to the local tilt given by the harmonic trap. This position given by $x_{\text{edge}} \simeq \Delta_0 a / V_0$ with $a = \lambda/2$ and $V_0 = \frac{1}{2}m(2\pi\nu a)^2$. By measuring the reflection point in lattices with different Δ_0 , we verify the relevant scaling $x_{\text{edge}} \propto \Delta_0$, as shown in Fig. S1. The blue line in Fig. S1A marks the theoretically expected x_{edge} with the uncertainty propagated from the uncertainty of the trap frequency ν . The disagreement between theory and experiment for larger values of Δ_0 can be explained by the finite waist of the lattice beams. In order to explore the edge in our system, the atoms are pumped by almost 100 unit cells ($\sim 100 \mu\text{m}$). Due to the Gaussian envelope of the transverse beams, which are essential to realise the pump, the lattice is effectively shallower far away from the centre. Thus, Δ_0 decreases towards the edge and atoms are reflected sooner.

We also find a small dependence of the reflection point on the pump period, compared to its absolute value, which spans roughly 10 unit cells when changing T from 2 ms to 10 ms (Fig. S1B). This can be understood by considering the energy spectrum of the Harper-Hofstadter-Hatsugai (HHH) model in a harmonic potential, which will be discussed below.

Experimental sequence

We start by preparing a degenerate cloud of fermionic ^{40}K in a crossed dipole trap. We have a spin mixture of $m_F = \{-9/2, -7/2\}$ except for the measurements in Fig. 2B and Fig. S1, where a spin-polarised cloud in the magnetic state $F = 9/2$, $m_F = -9/2$ is used. The spin-polarised cloud is directly loaded into the pumping lattice, while the spin mixture is first loaded into an intermediate chequerboard lattice with strongly attractive interactions. The two-step loading precludes the presence of atoms in the higher band and gives a larger fraction of atoms in doubly occupied unit cells [22].

After pumping the system for varying times, we either take a in-situ absorption image to measure the density or detect the band population with band-mapping. The latter is implemented with an exponential ramp to switch off the lattice beam in $500 \mu\text{s}$, followed by a time-of-flight expansion of 25 ms before absorption imaging.

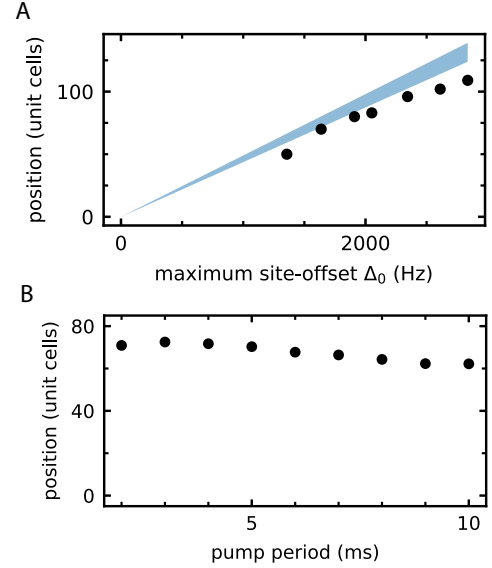


FIG. S1. Experimental dependence of the reflection position. The reflection point is expected to depend linearly on the maximal site-offset per pump cycle Δ_0 which is experimentally verified in (A). Deviations for large values of Δ_0 can be explained by the finite waist of the laser beams forming the lattice. (B) shows the period dependence of the reflection position. Changing the pump period T over an order of magnitude only changes the reflection point by about 10 unit cells, which is a result of the smooth boundary of a harmonic potential.

Realisation of a Thouless pump in the Rice-Mele model

The lattice setup is comprised of non-interfering standing waves in x , y , and z directions, together with interfering laser beams in the x - z plane. All the lattice beams come from a single laser source at wavelength $\lambda = 1064 \text{ nm}$. These potential combine to form a honeycomb lattice in the x - z plane, which can be considered as isolated tubes of one-dimensional superlattices along x in the limit of deep transverse lattices. In each 1D tube the potential can be modeled by a one-dimensional superlattice with two sites per unit cell. With this setup, we realise the Rice-Mele model [22]. In the tight-binding limit, the Rice-Mele model can be described with three numbers: the offset energy Δ between the two sites of a unit cell, the averaged nearest-neighbour tunneling t and the bond dimerisation δ which gives half the difference between the inter- and intra-dimer tunnellings. By having a dynamical control of the relative phase φ between the laser beams generating the interfering and the non-interfering lattice, we manage to shift the two with respect to each other. This shift modulates Δ and δ periodically, which can be depicted as a closed trajectory in the Δ - δ coordinate (Fig. S2). In the adiabatic limit, this realises a Thouless pump with its hallmark quan-

tised transport. In this case, the atomic displacement is given by the number of revolutions around the origin of the Δ - δ plane.

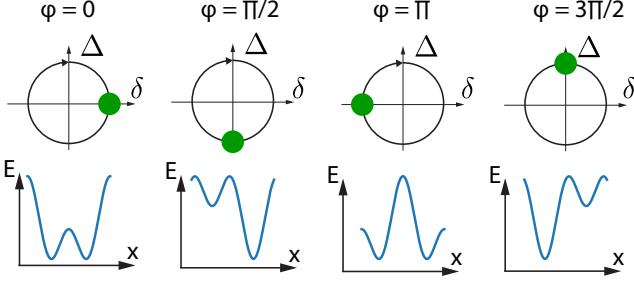


FIG. S2. **Realisation of a Thouless pump in the Rice-Mele model.** In our system the 1D lattice potential can be modelled by a superlattice with two sites per unit cell, which is depicted in the bottom part of this figure as a function of relative phase φ . The local site offset Δ as well as the bond dimerisation δ is depicted in the Δ - δ plots corresponding to the respective potentials. The resulting pump displacement corresponds to the number of revolutions around the origin in the Δ - δ plane.

Mapping a 1D Thouless pump to a 2D Hofstadter Model with quantum Hall response

A 1D Thouless pump with a period of T , as realised in our experiment, can be mapped to a 2D topological tight-binding (HHH) model with an applied electric field $E = \frac{2\pi\hbar}{qT}$ where q can be thought of as a fictitious charge of neutral atoms. Due to the topological bandstructure, this electric field leads to a transverse current $I_{\text{trans}} = \frac{q}{T}$ of one atom per period, when considering a fully occupied band. The 2D model therefore has a quantised transverse conductance $\sigma_{\text{trans}} = I_{\text{trans}}/E = \frac{q^2}{2\pi\hbar}$ analogous to the Hall conductance in the Quantum Hall Effect (QHE).

The time-periodicity of the Hamiltonian in Eq. 1 with $\hat{H}(\tau) = \hat{H}(\tau + T)$ allows us to use Floquet's theorem. Solutions of the time-dependent Schrödinger equation

$$i\hbar\partial_\tau |\Psi(\tau)\rangle = H(\tau) |\Psi(\tau)\rangle \quad (\text{S1})$$

can thus be written as

$$|\Psi(\tau)\rangle = e^{-i\epsilon\tau/\hbar} |u(\tau)\rangle \quad (\text{S2})$$

with $|u(\tau + T)\rangle = |u(\tau)\rangle$ and $\epsilon \in \mathbb{R}$. Due to the time-periodicity of $u(\tau)$ we expand it as a Fourier series,

$$|u(\tau)\rangle = \sum_n e^{-i\omega n\tau} |u_n\rangle, \quad (\text{S3})$$

where $\omega = 2\pi/T$ is the pump frequency. The change from the time-domain into the Fourier-domain is the key

ingredient to map the 1D Thouless pump to a 2D tight-binding model. The index n is also called the photon number of the mode $|u_n\rangle$.

Using a multi-index $\alpha = (j, \sigma)$ we write the T -periodic 1D Hamiltonian for $U = 0$ in the Fourier-basis:

$$\begin{aligned} \hat{H}(\tau) &= \sum_{\alpha, \beta} h_{\alpha\beta}(\tau) |\alpha\rangle \langle \beta| \\ &= \sum_{\alpha, \beta, m} e^{-im\omega\tau} h_{\alpha\beta}^m |\alpha\rangle \langle \beta| \end{aligned} \quad (\text{S4})$$

with $h_{\alpha\beta}^m = \frac{1}{T} \int_0^T e^{im\omega\tau} h_{\alpha\beta}(\tau) d\tau$ and $|\alpha\rangle$ corresponding to an atom localised on site j with spin σ . Likewise, we use Fourier decomposition to express the solutions to Eq. S1 as

$$|\Psi(\tau)\rangle = e^{-i\epsilon\tau/\hbar} \sum_{n, \alpha} e^{-in\omega\tau} u_{n, \alpha} |\alpha\rangle. \quad (\text{S5})$$

where $u_{n, \alpha} = \langle \alpha | u_n \rangle$. As a result, we obtain an eigenvalue equation for $u_{n, \alpha}$:

$$\epsilon u_{n, \alpha} = -n\hbar\omega u_{n, \alpha} + \sum_{\beta, m} h_{\alpha\beta}^m u_{n-m, \beta} \quad \forall n, \alpha \quad (\text{S6})$$

which can be understood as a time independent Schrödinger equation of a 2D tight-binding model with a tilted potential energy along one axis. By explicitly evaluating the $h_{\alpha\beta}^m$, we get

$$H_{2D} = H_{\text{real}} + H_{\text{synth}} + H_{\text{diag}} + H_V + H_{\text{tilt}}, \quad (\text{S7})$$

with

$$H_{\text{real}} = -t \sum_{j, n, \sigma} (\hat{c}_{j, n, \sigma}^\dagger \hat{c}_{j+1, n, \sigma} + h.c.), \quad (\text{S8})$$

$$\begin{aligned} H_{\text{diag}} &= -\frac{\delta_0}{2} \sum_{j, n, \sigma} e^{-i\pi j} (\hat{c}_{j, n, \sigma}^\dagger \hat{c}_{j+1, n+1, \sigma} \\ &\quad + \hat{c}_{j, n, \sigma}^\dagger \hat{c}_{j+1, n-1, \sigma} + h.c.), \end{aligned}$$

$$H_{\text{synth}} = -\frac{\Delta_0}{2} \sum_{j, n, \sigma} e^{-i\pi j} (i\hat{c}_{j, n, \sigma}^\dagger \hat{c}_{j, n+1, \sigma} + h.c.),$$

$$H_V = \sum_{j, n, \sigma} V(j) \hat{c}_{j, n, \sigma}^\dagger \hat{c}_{j, n, \sigma},$$

$$H_{\text{tilt}} = -\sum_{j, n, \sigma} \hbar\omega n \hat{c}_{j, n, \sigma}^\dagger \hat{c}_{j, n, \sigma}.$$

H_{real} and H_{synth} describe tunneling along the real (x) and synthetic (n) dimension, respectively.

The diagonal tunnelling terms in H_{diag} are crucial because they open a bandgap between the ground band and the first excited band, characterised by the topological Chern number C which is further related to the quantised Hall conductance via $\sigma_{\text{trans}} = \frac{q^2}{2\pi\hbar} C$. The terms in H_V

describe the external potential along the real-space direction. H_{tilt} corresponds to a linear tilt in potential energy along the synthetic dimension which can be thought of as originating from an electric field $E = \frac{2\pi\hbar}{qT}$ pointing along n .

Edge modes and their reflection properties

To illustrate the topological edge modes in the presence of an external potential, we evaluate the spectrum of H_{2D} in the adiabatic limit ($\omega \rightarrow 0$) for different potentials

$$V(j) = \frac{1}{2}m(2\pi\nu a)^2 j^\kappa \quad (\text{S9})$$

with m being the mass of ^{40}K , trap frequency $\nu = 134$ Hz, lattice spacing $a = 532$ nm, and lattice site j . The parameter κ , an even integer, characterises steepness of the trap; the limit $\kappa \rightarrow \infty$ corresponds to the textbook case of infinitely sharp walls [28]. Fig. S3A-C shows the numerically calculated energy spectra, omitting states on localised to the left edge for clarity.

Fig. S3A shows the spectrum for a box-like potential with $\kappa = 24$. In this case there is a family of topological edge states, marked in red, which connect the lower and the upper band (black), separated from topologically trivial states above 5 kHz (also in black). All red states are localised along the right edge in x -direction. The lower and upper band have Chern number 1 and -1 , respectively. Considering the dynamics in this model, an applied electric field along n as defined in H_{tilt} leads to Bloch oscillations with a period T along k_n . At the same time, the center-of-mass of the atoms moves by one unit cell per Bloch oscillation period along x , which corresponds to the quantised bulk Hall drift [14, 15]. This drift can be evaluated in the numerics by following the eigenstates in Fig. S3A in real space. Since the red edge states are gapped from the next higher-lying trivial (black) states, the atoms ‘Bloch-oscillate’ from the ground to the excited band via the red-marked edge modes over several periods. Once they are in the excited band they are transported backwards along x .

Fig. S3B shows the situation for $\kappa = 10$. It behaves similarly to Fig. S3A, except that there are more localised states marked in red, compared to $\kappa = 2$. Likewise, these states are transported along x as they undergo Bloch oscillations. As before, this family of edge states is gapped from trivial states and connects right-moving to left-moving states, which leads to the reflection phenomenon.

The experimentally relevant case is a harmonic trap with $\kappa = 2$ (see also refs. [23, 29–31]). Fig. S3C shows that for $\kappa = 2$ the number of localised states outside of the bands is even larger than for $\kappa = 10$. As before, we adiabatically follow these localised states along k_n

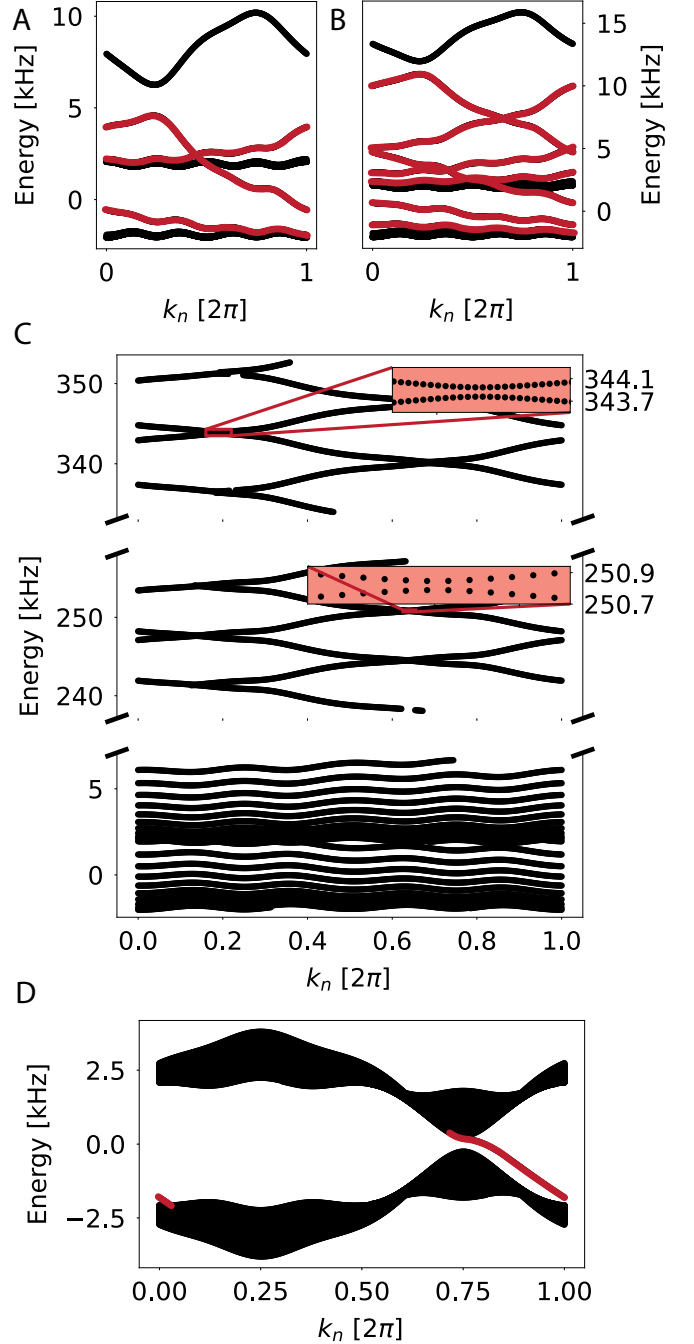


FIG. S3. **Energy spectra for different confining potentials.** States localised to the left edge are omitted for clarity. Energy spectra of H_{2D} in the limit $\omega \rightarrow 0$ for $\kappa = 24$ (A), $\kappa = 10$ (B), and $\kappa = 2$ (C). Topological edge modes which connect the two bands with Chern number 1 and -1 in (A) and (B) are marked in red. The upper inset in (C) marks the topological boundary where the reflection is observed as described in the main text. The inset in the center of (C) shows the tiny avoided crossings which can lead to a slight period dependence of the observed reflection point (Fig. S1). (D) Energy spectrum for a linearly increasing staggered potential. The gapless, topological edge mode is marked in red.

and evaluate their centre-of-mass along x . By numerically observing these drifts we confirm that the states describe quantised drifting in a large region, which manifests their nontrivial topological nature. Thus, the $\kappa = 2$ case is ideal to observe the reflection after long-distance quantised Hall drifts. However, the gaps between topological (right-moving and left-moving) and trivial (stationary) states become smaller, compared to the $\kappa = 24$ and $\kappa = 10$ cases, as shown in the insets of Fig. S3C ($\kappa = 2$). As a result, the reflection point for $\kappa = 2$ is spread out over several unit cells but the reflection itself remains intact. Faster pumping leads to non-adiabatic crossings of the energy gaps between right-moving and left-moving states, causing the reflection to happen later in time and further up in energy. We confirm this dependence experimentally in Fig. S1B, which shows a later reversal for smaller pump periods.

Fig. S3D shows the spectrum for the linearly increasing staggered potential, described in the following sections. This potential allows a straightforward identification of the gapless edge mode (red line). The states corresponding to this gapless edge mode are localised around the topological boundary.

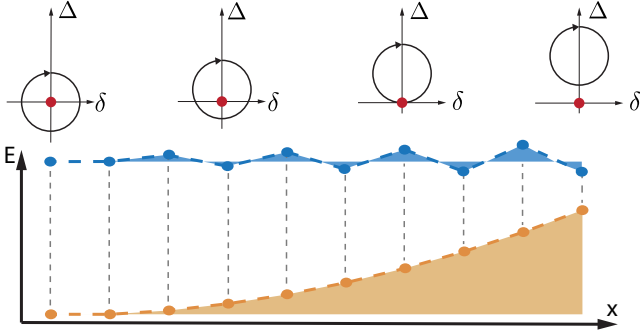


FIG. S4. **Linearly increasing staggered potential.** To elucidate the topology in our system, a linearly increasing staggered potential is considered (blue): $V(j) = jV_0(-1)^j$ with $V_0 = 1/2 \times m(2\pi\nu a)^2$, as before. It is chosen such that the local tilt always equals the tilt from the harmonic potential (orange), but alternates in sign. The staggered potential allows a simple pictorial representation of the emergence of the topological boundary. In a local density approximation the trap linearly shifts the pump trajectory upwards in the Δ - δ plane, as depicted in the upper part of the figure. As soon as the trajectory ceases to enclose the critical point, a topological-trivial boundary develops.

Staggered potential

Another possibility to identify the topological boundary in our system makes use of a staggered potential. First, we consider a potential with uniform staggering,

given by $V_c(j) = V(-1)^j$, where j indexes the lattice-site and $2V$ corresponds to the energy difference between adjacent sites. Adding such a potential to the Rice-Mele Hamiltonian (Eq. 1) changes its trajectory in the Δ - δ plane. The onsite energy in such a system is given by $(\Delta(\tau) + V)(-1)^j$, which ranges from $-\Delta + V$ to $\Delta + V$. The tunnellings are unchanged. Therefore, the trajectory remains circular and it is simply shifted upwards by an amount V .

A topological boundary emerges for a linearly increasing staggered potential, given by $V(j) = jV_0(-1)^j$, with $V_0 = \frac{1}{2}m(2\pi\nu a)^2$ as before. $V(j)$ is chosen such that it has the same local tilt as the harmonic trap in the experiment. Within the local density approximation we assign a Δ - δ trajectory locally to each unit cell. The trajectories are thus linearly shifted upwards as function of j (Fig. S4), describing a change of topology in real space. We expect the local density approximation to be valid since the atomic eigenstates in the experiment are strongly localised. Similar models with linearly increasing staggered potential have been studied in refs. [29, 32, 38].

Local Chern marker

The mathematical formulation of the Chern number as a topological invariant requires translational invariance, which does not apply to realistic experiments. Instead, we use a local quantity, known as Chern marker [8, 33]. The local Chern marker depends on the real-space position and it is defined by:

$$c(r_\gamma) = -\frac{4\pi}{A_c} \text{Im} \sum_{s=A,B} \langle r_{\gamma_s} | \hat{P} \hat{x} \hat{Q} \hat{y} \hat{P} | r_{\gamma_s} \rangle, \quad (\text{S10})$$

where r_γ is the position of the unit cell γ with sub-lattice-sites at positions r_{γ_A} and r_{γ_B} , $|r_{\gamma_s}\rangle = c_{\gamma_s}^\dagger |0\rangle$ is the state localised on the corresponding lattice site, A_c is the area of a real-space unit cell, $\hat{Q} = 1 - \hat{P}$ and \hat{P} is the projector onto the ground band. Defining \hat{P} is not unambiguously possible in our system (Eq. S7) because of the energy shift from the harmonic confinement. Instead, we use a linearly increasing staggered potential, as described in the previous paragraph. This model leaves the bands intact and a ground band can be unambiguously defined. Experimentally, a local probe of the band topology is the velocity of the Hall drift, plotted in Fig. 2A. Theory and experiment agree approximately with one another. The local velocity is extracted from the atomic positions by fitting linear functions to groups of three adjacent datapoints in ten pump cycles. The resulting velocities are plotted against position and smoothed through a running average of width three (ten cycles).